0 0 0 0 4 2 0 1 3 3 0

Submitted to Metallurgical
Transactions

LBL-3164
Preprint c.1

COMPARATIVE FRACTURE TOUGHNESS TESTING OF CRYOGENIC ALLOYS AT LIQUID HELIUM TEMPERATURE

Sungho Jin, S. K. Hwang and J. W. Morris, Jr.

August 1974

Prepared for the U. S. Atomic Energy Commission
under Contract W-7405-ENG-48

For Reference

Not to be taken from this room

LAWRENCE BERKELEY LABORATORY
UNIVERSITY OF CALIFORNIA
BERKELEY

LBL-3164
c.1

DISCLAIMER

This document was prepared as an account of work sponsored by the United States Government. While this document is believed to contain correct information, neither the United States Government nor any agency thereof, nor the Regents of the University of California, nor any of their employees, makes any warranty, express or implied, or assumes any legal responsibility for the accuracy, completeness, or usefulness of any information, apparatus, product, or process disclosed, or represents that its use would not infringe privately owned rights. Reference herein to any specific commercial product, process, or service by its trade name, trademark, manufacturer, or otherwise, does not necessarily constitute or imply its endorsement, recommendation, or favoring by the United States Government or any agency thereof, or the Regents of the University of California. The views and opinions of authors expressed herein do not necessarily state or reflect those of the United States Government or any agency thereof or the Regents of the University of California.

0 0 0 0 4 2 0 1 3 5 1

LBL-3164

COMPARATIVE FRACTURE TOUGHNESS TESTING OF CRYOGENIC ALLOYS AT LIQUID HELIUM TEMPERATURE

by

Sungho Jin, S. K. Hwang, and J. W. Morris, Jr.

Center for the Design of Alloys, Inorganic Materials Research Division
Lawrence Berkeley Laboratory, University of California
Berkeley, California 94720

ABSTRACT

Fracture behavior of the Fe-12Ni-0.25Ti alloy grain refined through thermal cycling was studied down to liquid helium temperature using a simple method of cryogenic fracture toughness testing. Comparision tests were also made with two other common cryogenic alloys.

Ultrafine grained Fe-12Ni-0.25Ti alloy, which is 100% ferritic, behaved in a ductile manner similar to 304 austenitic steel. It was shown that the ductile-brittle transition temperature of the ferritic steel specimen can be suppressed below liquid helium temperature by grain refinement even in the presence of a sharp crack. Yield strength of 149 ksi with fracture toughness of 307 ksi$\sqrt{in}$ at liquid nitrogen temperature, and yield strength of 195 ksi with fracture toughness of 232 ksi$\sqrt{in}$ at liquid helium temperature were obtained.

Sungho Jin is Assistant Research Engineer, S. K. Hwang is Graduate Student Research Assistant, and J. W. Morris, Jr. is Associate Professor of the Department of Materials Science and Engineering, University of California, Berkeley, California 94720.

I. INTRODUCTION

This paper reports a continuation of previous research on Fe-12Ni-0.25Ti cryogenic alloy system.[1] We have previously described an alternate thermal cycling method of grain refinement which yields a 0.5-2μm grain diameter and causes a significant improvement in cryogenic fracture toughness. The ductile-brittle transition temperature of this completely ferritic alloy in Charpy impact testing was suppressed below liquid helium temperature. A compact tension fracture toughness test of the alloy at liquid nitrogen temperature showed a fracture mode of completely ductile dimple rupture without any unstable crack propagation.

In this paper the fracture behavior of the grain refined Fe-12Ni-0.25Ti alloy was investigated at liquid helium temperature using a simple test method recently developed in this laboratory. Comparison tests were performed with commercial 9-Ni steel (containing 4 ∿ 6% retained austenite) and 304 stainless steel (100% austenitic) at liquid nitrogen (77°K) and liquid helium temperature (∿ 6°K).

II. EXPERIMENTAL PROCEDURES

Chemical compositions of the three alloys investigated are shown in Table I. The Fe-12Ni-0.25Ti alloy was prepared by induction melting in an argon gas atmosphere. Twenty-pound ingots were homogenized under vacuum at 1050°C for 120 hours, and cross forged at 1100°C to thick plates 10 cm wide by 1.9 cm thick. These plates were annealed at 900°C for two hours to remove prior deformation strain, then air cooled to room temperature. The starting material has a grain size of 40 ∿ 60 μm. Grain refinement was performed through alternate thermal cycling[1] in the γ and $(\alpha + \gamma)$ range with intermediate air cooling as shown in Fig. 1. (The specimen after the first thermal cycling step was labelled 1A, and after the final fourth step as 2B.) The 9-Ni steel and the 304 stainless steel were procured commercially. The 9Ni steel was tested as received (double normalized and tempered). The 304 stainless steel was annealed at 1020°C for one hour and ice brine quenched.

Cryogenic tensile tests were conducted at 77°K and at 4.2°K using an Instron machine equipped with suitable cryostats. Subsize specimens of 12.7 mm gauge length and 3 mm gauge diameter were tested at a crosshead speed of 0.05 cm/min.

Fracture toughness tests were conducted at 77°K on an MTS Universal Testing Machine equipped with a liquid nitrogen cryostat. The test specimens were compact tension (WOL) specimens of 17.8 mm thickness(B), 50.8 mm width(W) and 25.4 mm crack length(a), machined with the rolling direction perpendicular to the loading direction and fatigue pre-cracked according to the ASTM specifications.[2]

Fracture toughness tests were conducted at liquid helium temperature using a new and simple method which avoids the need for elaborate cryostat systems. A "boxing technique" similar to that used in Charpy V-notch impact testing at liquid helium temperature[3] was employed. A 0.6 mm diameter hole was drilled to the center of the compact tension fracture toughness specimen ∿ 13 mm below the fatigue crack tip. A plastic tube (thermocouple protection tube) of 1.6 mm inside diameter and 12.7 mm length was glued firmly onto this hole. The specimen was covered with grooved styrofoam (2.5mm thick), and the surface of the styrofoam was then wrapped with Scotch tape. The insulated specimen was inserted into a rectangular lucite box of 0.8 mm wall thickness as shown in Fig. 2. As shown in the figure the lucite box contains several holes: there are two ovular holes for the pins to go through the specimen and the MTS grips, a 9.8 mm diameter hole on which the polyethylene inlet pipe is glued, a 3 mm diameter hole through which the thermocouple protection tube passes, and a rectangular hole through which the clip-in strain gauge is installed. This last opening also serves as an exit for the liquid and evaporated helium. The completed system was inserted into the MTS grips we used as shown in Figs. 3 and 4. Oversize grips of 25.4 mm inside width are used. A thermocouple (Gold-Chromel) was inserted through the protection tube and then fixed with glue to the protection tube. The thermocouple is in close contact with the metal at the center of the specimen thickness, but is insulated from the liquid helium. A strain clip gauge was installed in the specimen and a thin layer of mylar was provided to prevent disturbance of the strain gauge by the cold helium vapor. The liquid helium

transfer line was inserted into the inlet pipe of the box.

Figures 5(a) and (b) illustrate the testing procedure. At a dewar pressure of 6 psi (4.2×10^4 N/m^2), a specimen temperature of 5 $\sim$ 6°K is obtained less than 3 $\sim$ 4 minutes after the transfer of liquid helium is initiated. This steady state temperature is maintained as long as liquid helium transfer is continued. A typical temperature-time curve is shown in Fig. 6. Liquid helium consumption was approximately 5 $\sim$ 7 liters for each fracture toughness test. The lucite box remains intact during the test. The box can be broken if it is necessary to break the specimen into halves.

Fracture surfaces of the broken fracture toughness specimens were examined in a Jeolco JSM-U3 Scanning Electron Microscope. Quantitative measurement of the amount of the retained austenite was made using a Picker X-ray Diffractometer with a Cu_{K_α} source.

III. RESULTS AND DISCUSSIONS

1. Microstructures

Details of the microstructural changes accompanying the alternate thermal cycling of the Fe-12Ni-0.25Ti alloys and their phase transformation behavior have been reported previously.[1] The optical microstructures of the alloys studied here are shown in Fig. 7 (a) through (d). The grain size and the phase distribution of these alloys are summarized in Table II.

2. Cryogenic Tensile Properties

The engineering stress-strain curves obtained in tensile tests at 77°K and at 4.2°K are shown in Fig. 8. The tensile properties measured at 77°K and 4.2°K are summarized in Table III. Some of these results have been published previously[1,6] but are reproduced here for completeness. At liquid helium temperature, the anticipated large increase in yield strength was observed for the Fe-Ni-Ti alloys and the 9-Ni steel.

The serrated yielding behavior observed at liquid helium temperature is common in many alloy systems including most Fe-base alloys. Among the several suggested explanations,[4] adiabatic heating during deformation[5] appears the most likely cause for the discontinuous yielding of the Fe-12Ni-0.25 Ti alloys. Both alloys 1A and 2B were completely martensitic before testing,[1] and no evidence of twinning was observed during the test. Each step of discontinuous yielding was accompanied by a sudden rise of specimen temperature.

3. Cryogenic Fracture Toughness

Fracture Toughness at 77°K

The results of the compact tension fracture toughness testing of the four alloys at 77°K are shown in Fig. 9 as load-crack opening displacement (COD) curves. None of the specimens were in the plane-strain condition at this temperature, and valid K_{IC} values (according to the ASTM specification[2]) could not be obtained with the given specimen thickness. However the relative fracture behavior can be clearly seen from the load-COD curves. In specimens of Fe-Ni-Ti(1A) and 9-Ni steel, unstable crack propagation could not be prevented; it is marked by the sudden drop of load in the load-COD curves. The ultrafine grained Fe-Ni-Ti(2B) and austenite 304 stainless steel were, however, immune to unstable crack propagation. The pre-induced fatigue crack grew slowly in a stable manner until the test was terminated. The ferritic Fe-Ni-Ti(2B) specimen behaved in a ductile manner, as did austenitic 304 stainless steel, however the 2B alloy has a much higher load carrying capacity. The post-test specimens are compared in Fig. 11(a). Scanning electron fractographs taken from the fracture surfaces showed a quasi-cleavage fracture mode for Fe-Ni-Ti(1A) and 9-Ni steel, but complete ductile dimple rupture for Fe-Ni-Ti(2B).[1]

Recent developments in elastic-plastic fracture theories, i.e., the J-integral concept[7,8] and the Equivalent Energy approach[9,10] allow the evaluation of fracture toughness from nonlinear load-displacement curves. Lower-bound fracture toughness of the alloys tested here was calculated according to Witt's Equivalent Energy theory,[10]

$$K_{IC} = \frac{P_Q \sqrt{A_1/A_2} \quad f(^a/W)}{B\sqrt{W}} \qquad \ldots\ldots(1)$$

where a, W, B refer to specimen crack length, width and thickness, and where P_Q is the 5% secant load defined by ASTM specification[2], $f(^a/W)$ is a known geometric shape factor[2], A_1 is the area under the load-displacement curve up to the maximum load, and A_2 is the area under the curve to the load P_Q. The results of the calculations are shown in Table IV. Each datum represents the average of three tests. Scattering of data was approximately $\pm$ 15 ksi$\sqrt{in}$. Calculations based on the J-Integral concept gave similar values for the fracture toughness.

Fracture Toughness at $6^{o}K$

Fracture toughness tests were conducted near liquid helium temperature (at $6^{o}K$) using the method described above. The results of the tests are shown in Fig. 10. Specimens of the Fe-Ni-Ti(1A) and the 9-Ni steel satisfied the ASTM thickness requirement for plane-strain conditions at this temperature and valid K_{IC} values were obtained. The fracture surfaces were completely flat with virtually no shear lips, as can be seen from the photograph of post-test specimens presented in Fig. 11(b). In these specimens the crack propagated with a repeated serration until final fracture.

Specimens of the 304 stainless steel also had flat fracture surfaces as if they were in a plane-strain condition, but these speciemns showed extended load-displacement traces (Fig. 10) and do not meet the ASTM thickness requirement. The crack grew slowly and steadily with very small amplitude of serration, and no"pop-in" occurred. The fracture surfaces and nearby areas are magnetic after the test, indicating transformation of austenite to martensite during fracture and accompanying plastic deformation.

Specimen 2B of the Fe-Ni-Ti alloy showed a much higher load carrying capacity at $6^{o}K$ than any other alloy tested, as can be seen in Fig. 10. The serration of the load-displacement curve up to the maximum load (and possibly beyond that point) does not necessarily mean a brittle or unstable crack propagation since the slip or yielding near this temperature also occurs in a discontinuous manner (as shown in Fig. 8). Comparing the post-test specimens broken at $6^{o}K$, Fig. 11(b), the large plastic zone size and the high

REFERENCES

1. S. Jin, J. W. Morris, Jr. and V. F. Zackay: Met. Trans., accepted for publication.
2. 1973 Book of ASTM Standard, Part 31, E 399-72, pp. 960.
3. S. Jin, W. A. Horwood, J. W. Morris, Jr., and V. F. Zackay: Advances in Cryogenic Engineering, 1974, vol. 19, pp. 373.
4. E. B. Kula and T. S. DeSisto: Amer. Soc. Testing Mater., Spec. Tech. Publ. 387, 1965, pp.1.
5. Z. S. Basinski: Proc. Royal Soc. London, 1957, vol. 240, pp. 229.
6. S. Jin, J. W. Morris, Jr., and V. F. Zackay: Advances in Cryogenic Engineering, 1974, vol. 19, pp. 379.
7. J. R. Rice, P. C. Paris, and J. G. Merkle: Amer. Soc. Testing Mater., Spec. Tech. Publ. 536, 1972, pp. 231.
8. J. A. Begley and J. D. Landes: Amer. Soc. Testing Mater., Spec. Tech. Publ. 514, 1972, pp.1.
9. P. C. Riccardella and J. L. Sweldow: WCAP-8224, Oct. 1973.
10. F. J. Witt and T. R. Mager: ORNL-TM-3894, Oct. 1972.

Table I. Chemical Compositions
(w.t. %)

	Fe	Ni	Ti	Cr	Mn	C	N	S	P
Fe-12Ni-0.25Ti	Bal	12.07	0.26	-	-	0.001	0.014	0.004	0.003
9-Ni Steel	Bal	8.94	-	-	0.41	0.090	-	0.008	0.006
304 Stainless	Bal	8.84	-	18.46	-	0.050	-	0.026	0.004

Table II. Grain Size and Phase Stability

	Fe-Ni-Ti(1A)	Fe-Ni-Ti(2B)	9-Ni-Steel	304 Stainless
Grain Size, um	10 ∿ 15	0.5 ∿ 2	10 ∿ 15*	70 ∿ 80
Vol. Pct. Austenite	0	0	4 ∿ 6	100

*With smaller grains (0.5 ∿1 um in diameter) located at the prior austenite boundaries.

Table III. Cryogenic Tensile Properties

	Alloy	Y.S.* ksi	U.T.S.** ksi	Elong. pct.	R.A. pct.
77°K	Fe-Ni-Ti(1A)	134	142	31.1	73.8
	Fe-Ni-Ti(2B)	149	154	26.8	72.1
	9-Ni steel	146	172	29.6	66.8
	304 stainless	81	235	47.3	65.6
4.2°K	Fe-Ni-Ti(1A)	182	207	23.8	72.9
	Fe-Ni-Ti(2B)	195	219	19.3	69.8
	9-Ni steel	208	231	21.2	59.1
	304 stainless	105	270	41.6	52.7

* At 77°K, 0.2 percent offset yield strengths were taken. At 4.2°K, the first discontinuous yield points were used.

** Ultimate tensile strengths at 4.2°K were obtained from the upper locus of discontinuous peaks in stress-strain curves.

† To convert to SI unit, 1 ksi = 6.89×10^6 N/m^2.

Table IV Fracture Toughness at Cryogenic Temperatures

	K_{IC} at $77^{o}K$ ksi$\sqrt{in}$	K_{IC} at $6^{o}K$ ksi$\sqrt{in}$
Fe-Ni-Ti(1A)	187*	75 (valid K_{IC})
9-Ni steel	168*	73 (valid K_{IC})
Fe-Ni-Ti(2B)	307*	232*
304 stainless	213*	168*

* Values calculated using Equivalent Energy concept, equation (1).

† To convert to SI units, 1 ksi $\sqrt{in}$ = 1.09×10^{6} $N/m^{2} \cdot \sqrt{m}$.

FIGURE CAPTIONS

Fig. 1 - Thermal cycling procedure of grain refinement in an Fe-12Ni-0.25 Ti alloy.

Fig. 2 - Lucite box for compact tension fracture toughness testing at liquid helium temperature.

Fig. 3 - Schematic illustration of the testing method at liquid helium temperature (front view).

Fig. 4 - Schematic illustration of the testing method at liquid helium temperature (side view).

Fig. 5 - Procedures for fracture toughness testing at liquid helium temperature. (a) Insulated specimen, liquid helium transfer line, clip-in displacement gauge, and thermocouple are properly arranged. (b) Liquid helium transfer is initiated and the test starts.

Fig. 6 - Change of specimen temperature as a function of time after the transfer of liquid helium was initiated.

Fig. 7 - Optical microstructures of the alloys tested. (a) Fe-Ni-Ti(1A) (b) Fe-Ni-Ti(2B), (c) 9-Ni steel, (d) 304 stainless steel.

Fig. 8 - Engineering stress-strain curves of the cryogenic tensile tests.

Fig. 9. - Load-crack opening displacement curves at 77°K.

Fig. 10 - Load-crack opening displacement curves at 6°K.

Fig. 11 - Post-test compact tension fracture toughness specimens. (a) at 77°K, (b) at 6°K.

Fig. 12 - Scanning electron fractographs taken from the fracture surfaces of the compact tension specimens tested at 6°K.

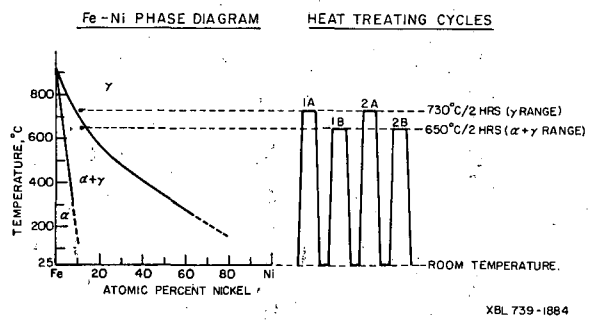

Fig. 1 - Thermal cycling procedure of grain refinement in an Fe-12Ni-0.25 Ti alloy.

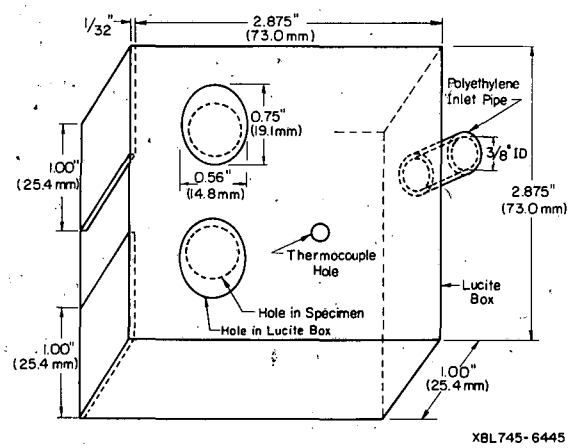

Fig. 2 - Lucite box for compact tension fracture toughness testing at liquid helium temperature.

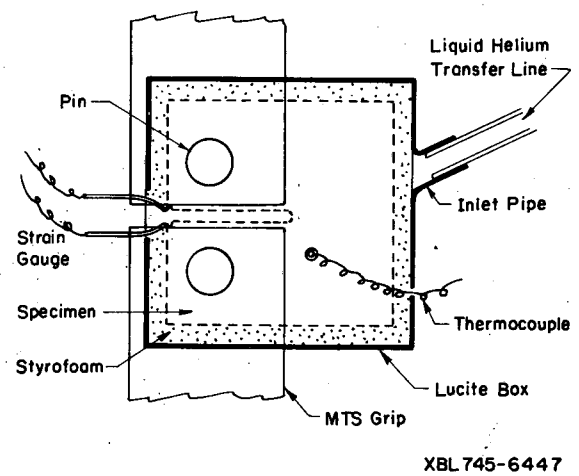

Fig. 3 - Schematic illustration of the testing method at liquid helium temperature (front view).

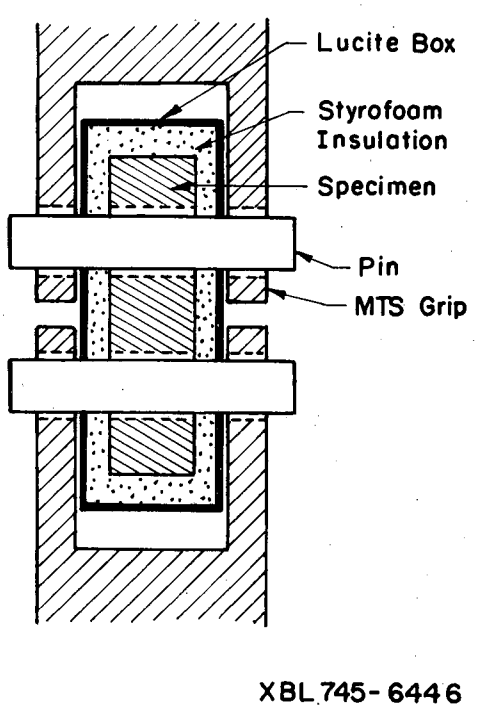

Fig. 4 - Schematic illustration of the testing method at liquid helium temperature (side view).

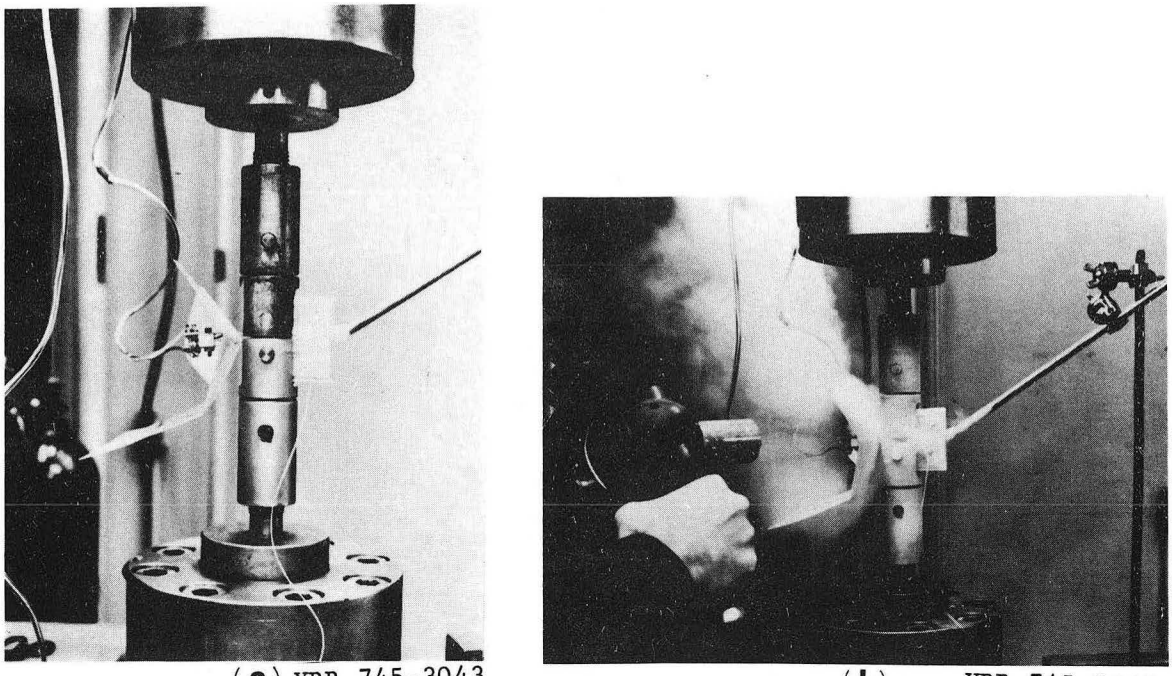

(a) XBB 745-3043 (b) XBB 745-3044

Fig. 5 - Procedures for fracture toughness testing at liquid helium temperature. (a) Insulated specimen, liquid helium transfer line, clip-in displacement gauge, and thermocouple are properly arranged. (b) Liquid helium transfer is initiated and the test starts.

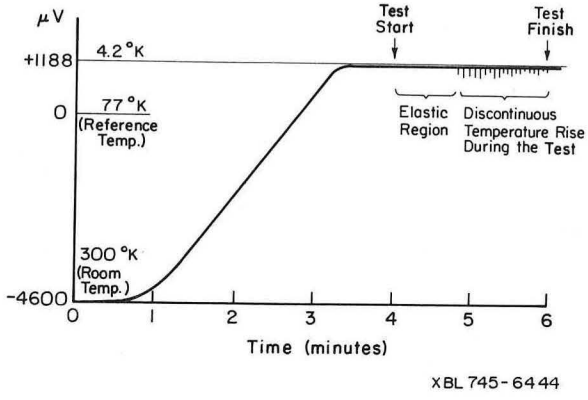

Fig. 6 - Change of specimen temperature as a function of time after the transfer of liquid helium was initiated.

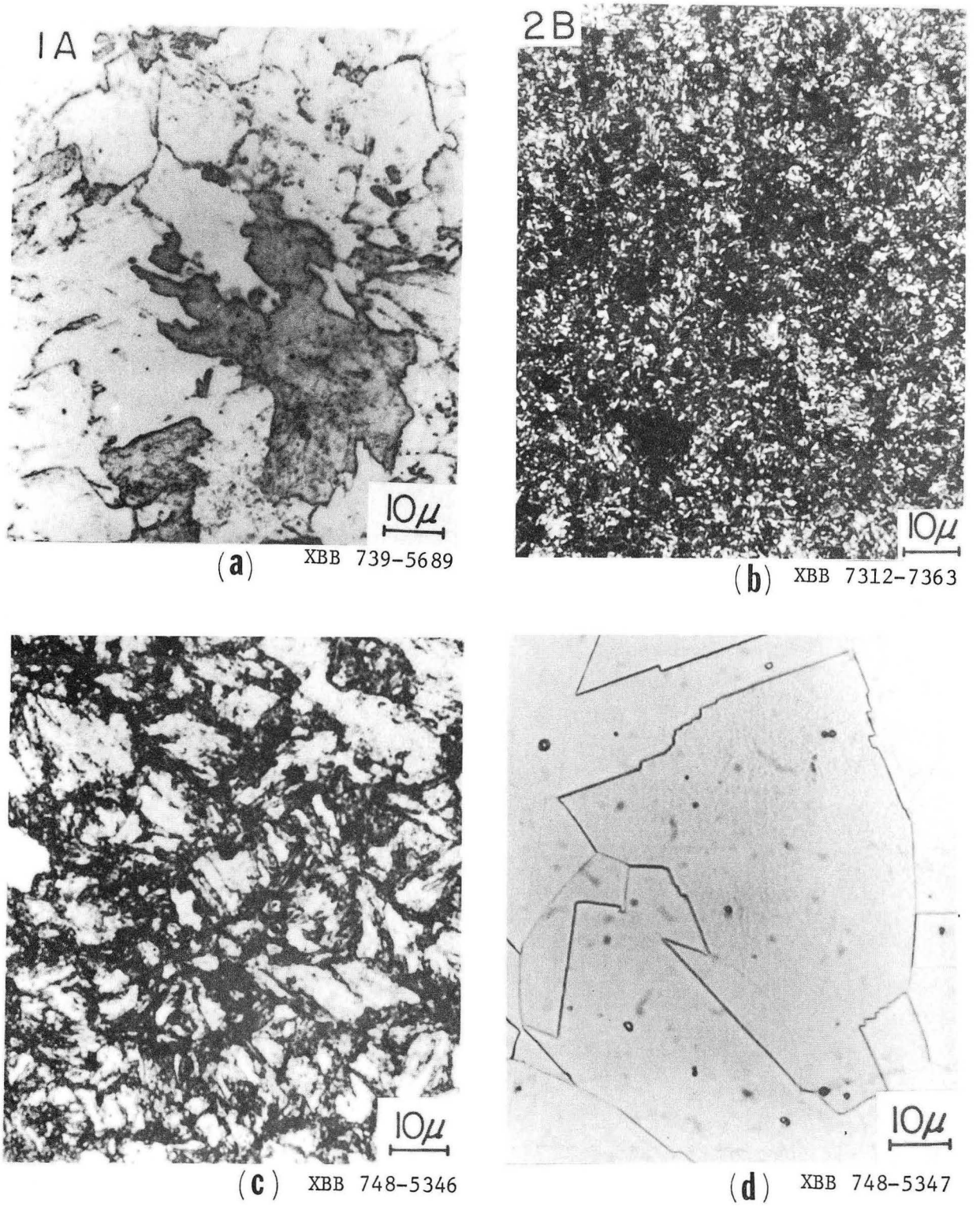

Fig. 7 - Optical microstructures of the alloys tested. (a) Fe-Ni-Ti(1A) (b) Fe-Ni-Ti(2B), (c) 9-Ni steel, (d) 304 stainless steel.

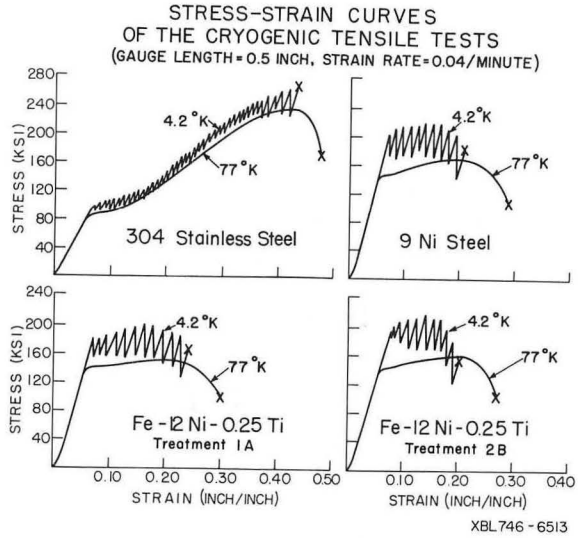

Fig. 8 - Engineering stress-strain curves of the cryogenic tensile tests.

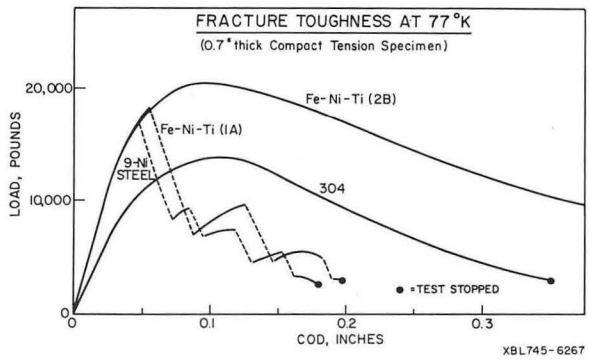

Fig. 9. - Load-crack opening displacement curves at 77°K.

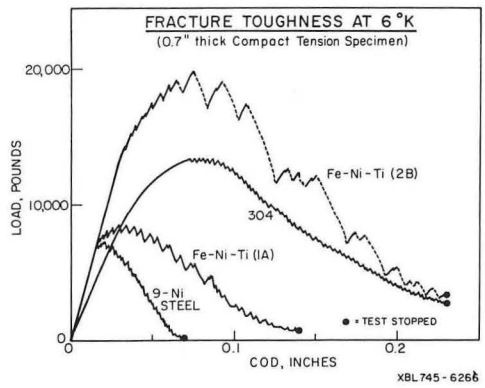

Fig. 10 - Load-crack opening displacement curves at 6°K.

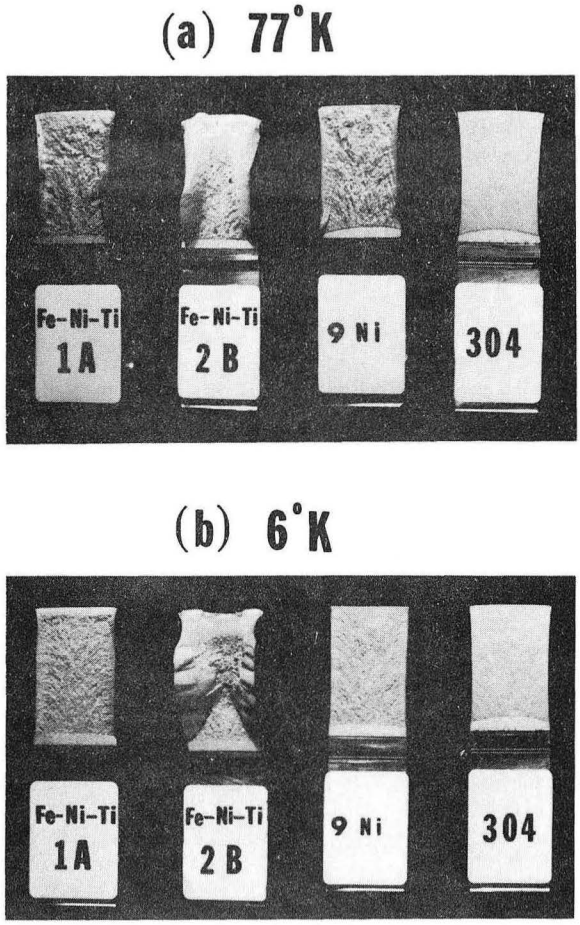

XBB 745-3045

Fig. 11 - Post-test compact tension fracture toughness specimens. (a) at 77°K, (b) at 6°K.

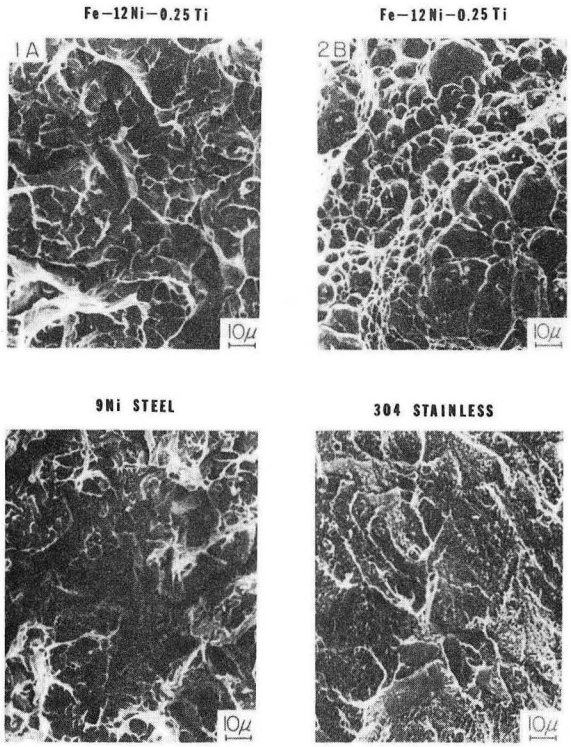

XBB 745-2982

Fig. 12 - Scanning electron fractographs taken from the fracture surfaces of the compact tension specimens tested at 6°K.

0 0 0 0 4 2 0 1 3 6 3

LEGAL NOTICE

This report was prepared as an account of work sponsored by the United States Government. Neither the United States nor the United States Atomic Energy Commission, nor any of their employees, nor any of their contractors, subcontractors, or their employees, makes any warranty, express or implied, or assumes any legal liability or responsibility for the accuracy, completeness or usefulness of any information, apparatus, product or process disclosed, or represents that its use would not infringe privately owned rights.

TECHNICAL INFORMATION DIVISION
LAWRENCE BERKELEY LABORATORY
UNIVERSITY OF CALIFORNIA
BERKELEY, CALIFORNIA 94720